Superlattices and Microstructures 99 (2016) 192–196

Contents lists available at ScienceDirect

Superlattices and Microstructures

journal homepage: www.elsevier.com/locate/superlattices

Low temperature iron gettering by grown-in defects in p-type Czochralski silicon

Haiyan Zhu, Xuegong Yu*, Xiaodong Zhu, Yichao Wu, Jian He, Jan Vanhellemont [1], Deren Yang**

State Key Laboratory of Silicon Materials and Department of Materials Science and Engineering, Zhejiang University, Hangzhou, 310027, PR China

ARTICLE INFO

Article history:
Received 22 December 2015
Accepted 5 March 2016
Available online 8 March 2016

Keywords:
Czochralski silicon
Iron gettering
Grown-in defect

ABSTRACT

Low temperature iron gettering in as-grown boron doped Czochralski silicon (Cz-Si) at temperatures between 220 and 500 °C is studied using microwave-photoconductive decay based minority carrier lifetime measurements. Scanning infrared microscopy technique is used to study the defect density/size distribution in the samples before and after anneal. It is found that the decrease of interstitial iron (Fe_i) concentration shows a double exponential dependence on annealing time at all temperatures. This suggests the existence of two sinks for Fe_i. Meanwhile, the observed bulk defect densities and sizes in contaminated and as-grown samples are nearly the same, implying that the grown-in defects could be the gettering centers in this process. The results are important for understanding and controlling low temperature Fe_i gettering during processing of Cz-Si based devices.

1. Introduction

Iron is one of the most prevalent impurities in silicon due to the wide use of stainless steel equipment in the fabrication line. It can remarkably degrade device performance due to the deep levels introduced by its isolated atoms, point defect complexes and precipitates [1–3]. In order to significantly improve the electronic material properties and device performance, a reduction of the interstitial iron (Fe_i) concentration is often beneficial.

Iron gettering technique has for that reason been extensively investigated from an engineering and scientific viewpoint [4–9]. In order to implement gettering procedures during device processing, the various mechanisms of iron precipitation as well as the strength and stability of gettering sites should be understood and quantified. The precipitation of Fe_i in float zone silicon (Fz-Si) is reported as a Fe_i diffusion limited process and the maximum precipitation occurs in the temperature interval of 500–600 °C [10], while the precipitation of Fe_i in Czochralski silicon (Cz-Si) that contains oxide precipitates is revealed to be a heterogeneous process, controlled by Ham's law [11,12]. A chemical rate equation model was proposed to describe the high temperature Fe_i gettering process in Cz-Si [13,14]. Despite the large number of studies, iron gettering in as-grown Cz-Si at temperatures below 500 °C, has hardly been reported on and the gettering mechanism -if any-has sill to be revealed.

* Corresponding author.
** Corresponding author.
E-mail addresses: yuxuegong@zju.edu.cn (X. Yu), mseyang@zju.edu.cn (D. Yang).
[1] On Leave from Department of Solid State Sciences, Ghent University, Belgium.

http://dx.doi.org/10.1016/j.spmi.2016.03.006
0749-6036/

In the present work, first results are presented of a study of Fe_i gettering in as-grown p-type Cz-Si at low temperatures in the range between 220 and 500 °C. As shown below, the observed gettering kinetics are described well by a double exponential dependence on annealing time which has never been reported before.

2. Experimental

150 mm diameter, 1–2 Ω cm, boron doped ⟨100⟩ Cz-Si wafers are cut into rectangular samples ($2 \times 2 \times 0.1$ cm^3). The samples are all from the comparable inner position of the wafers. The interstitial oxygen concentration of the samples is in the range of $8–11 \times 10^{17}$ cm^{-3}, as determined by fourier-transform infrared (FTIR) spectroscopy using the IOC-88 calibration coefficient of 3.14×10^{13} cm^{-2}. The samples are immersed into a 0.1 mol/L ferric nitric acid ($Fe(NO_3)_3$) solution for 15 min to form a source of iron contamination on both sample surfaces. After drying, iron is driven-in by annealing in argon ambient at 850 °C for 170 min, followed by quenching in methyl silicone oil. This step ensures that the interstitial iron atoms diffuse through the whole wafer thickness thus leading to a relatively uniform Fe_i concentration of about 3×10^{13} cm^{-3}, corresponding well with the reported solubility of interstitial iron at 850 °C [1]. After the drive-in, a 50 μm iron rich layer is removed from both surfaces of the samples by chemical etching in a 3:1 solution mixture of HNO_3 and HF for 2 min. In order to reduce the surface recombination to a minimum, the samples are passivated by a 110 nm plasma enhanced-chemical-vapour-deposited (PECVD) silicon nitride layer on both surfaces.

The samples are then annealed between 220 and 500 °C for up to 60 h. After each anneal step, the sample is stored in dark at 50 °C for 1 h to allow pairing of all the remaining Fe_i with B. The evolution of minority carrier lifetime with illumination time is measured at three locations on each sample using microwave-photoconductive decay (μPCD), with a 904 nm pulse laser supplying the energy to gradually dissociate the formed FeB pairs. A complete FeB pair dissociation is realized by illuminating for more than 30 min when the carrier lifetime becomes stable. By the relative change in lifetime, quantitative assessment of the Fe_i concentration is made using the empirical equation [15].

$$[Fe_i] = C\left(1/\tau_{initial} - 1/\tau_{final}\right), \quad (1)$$

whereby C depends on the excitation level and the dopant concentration. In the present work $C = 3.4 \times 10^{13}$ is used. $\tau_{initial}$ and τ_{final} are the lifetimes before and after dissociation of FeB pairs.

After the final annealing step, the passivation layers are removed by etching in 10% HF solution. Size and density of the bulk defects in all contaminated samples as well as a reference sample without contamination and anneals are examined by scanning infrared microscopy (SIRM) using the 980 nm wavelength laser of a SIRM-300 instrument of Semilab.

3. Results and discussions

Fig. 1 shows a comparison of the carrier lifetime maps of Fe indiffused samples before and after anneals at 220, 300, 400 and 500 °C, illustrating that in all cases the average lifetime is increased by annealing. With a similar initial average lifetime of about 0.8 μs, the samples show improved lifetimes of 1.2 μs (220 °C/60 h), 1.6 μs (300 °C/60 h), 3.2 μs (400 °C/1280 min) and 3.5 μs (500 °C/320 min), respectively. All the lifetime maps are measured after complete formation of FeB pairs, therefore the

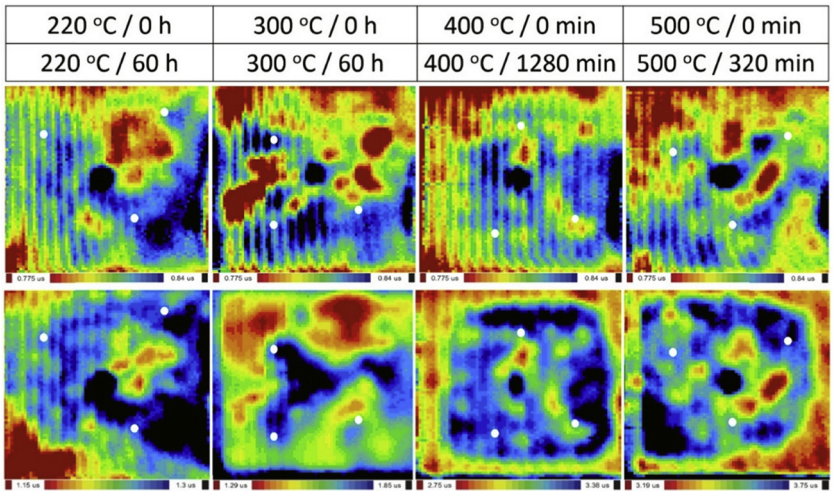

Fig. 1. Lifetime maps of Fe indiffused samples before (top) and after (bottom) low temperature annealing. The data used in Fig. 3 were obtained at three locations on each sample, indicated by the white dots.

measured lifetimes allow estimating the FeB pair concentration and thus also the Fe_i concentration differences between the samples. A higher lifetime indicates a stronger reduction of Fe_i concentration by gettering or precipitation during the anneal.

It can be seen that the lifetimes are quite constant across each sample, indicating a relatively uniform Fe_i concentration distribution. In order to minimize the error, three positions with similar lifetimes, i.e. with close Fe_i concentration, are chosen to do the laser illumination for the lifetime measurement. These locations are indicated in Fig. 1 with the white dots. Since the lifetime evolution at each spot is measured one by one, the three spots should be separated to avoid dissociation of FeB pairs at the next spot when illuminating the present one.

Fig. 2 shows the evolution of carrier lifetime with illumination time of different Fe indiffused samples before and after low temperature anneal. The initial value of each curve is in agreement with the average lifetime of the maps in Fig. 1, indicating that the measured positions are representative for the whole wafer. One can observe that the lifetime increases rapidly at first and finally reaches a saturation value corresponding to the complete dissociation of FeB pairs. The increase of initial lifetime after annealing is due to the reduction of Fe_i concentration. The curves before and after annealing at 220 °C are very close (see Fig. 2(a)), implying the gettering efficiency of this very low temperature thermal treatment is not high. Annealing at 300 °C or higher, the difference between the two curves becomes larger, indicating that more iron is gettered during the anneal. Comparing the annealed curves in Fig. 2(c) and (d), one can observe that the Fe_i concentrations are reduced to the same level, but the required annealing time at 500 °C is much shorter illustrating that the gettering efficiency at 500 °C is higher than that at 400 °C.

The remaining Fe_i concentration after each annealing step is determined by the initial and final carrier lifetimes extracted from the lifetime vs. time curves, using Equation (1). The points in Fig. 3 shows the dependence on the annealing time at different temperatures of the normalized fraction of the remaining Fe_i concentration. The observed Fe_i gettering kinetics cannot be fitted well with a single exponential as would be expected when the behavior was in agreement with the theory of Ham. Fitting with a double exponential

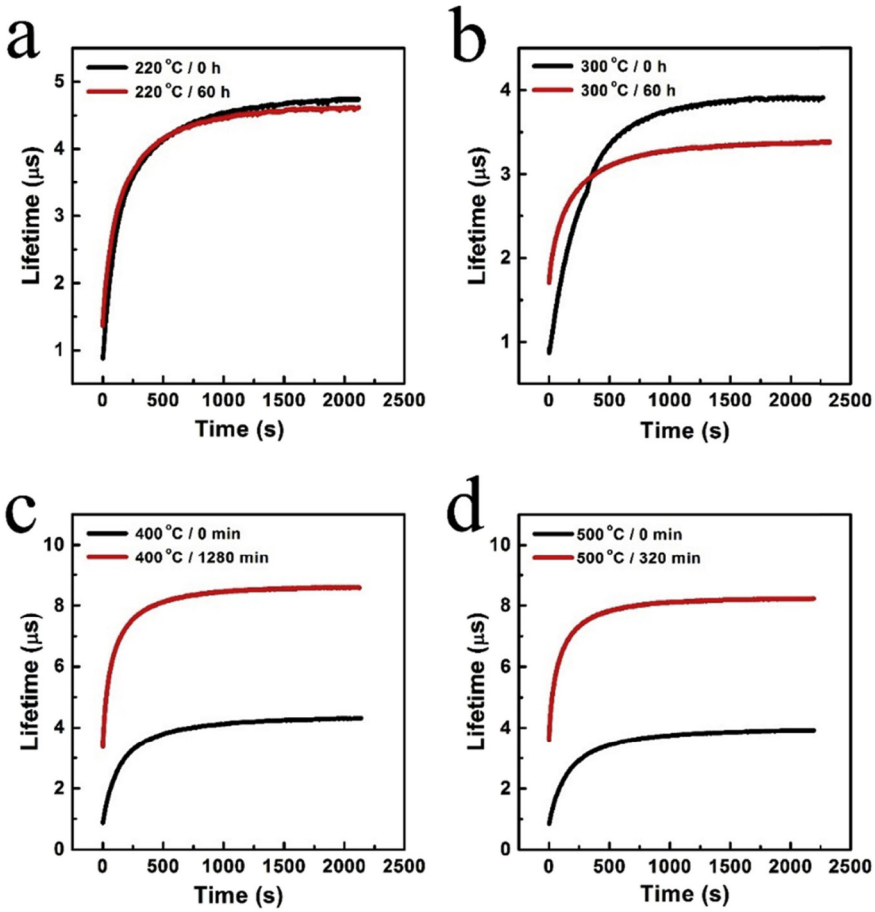

Fig. 2. The evolution of minority carrier lifetime with illumination time for Fe indiffused samples before and after the low temperature anneal. The lifetime-time curves are similar at the three measured locations on each sample.

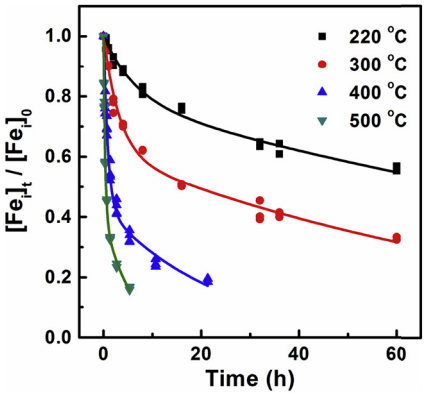

Fig. 3. Measured normalized interstitial iron concentration as a function of annealing time at different temperatures. The full lines are best fits using Equation (2).

$$[Fe_i](t)/[Fe_i](0) = A\exp(-t/\tau_1) + (1-A)\exp(-t/\tau_2), \quad (2)$$

allows however to reproduce very well the experimental data for all temperatures as illustrated in Fig. 3 by the solid lines. The results of the fitting are listed in Table 1.

t is the annealing time, $[Fe_i](t)$ is the Fe_i concentration after the annealing time t, $[Fe_i](0)$ is the initial Fe_i concentration, τ_1 and τ_2 are the characteristic decay constants, and A is a fitting factor indicating the ratio of the two parts.

The excellent fits suggest that the gettering process is governed by two Fe_i sinks during the low temperature annealing. As can be seen from Table 1, the fitting factor A decreases with increasing annealing temperature, implying the second exponential decay characterized by τ_2 becomes more and more important with increasing temperature. One can also notice that at each temperature τ_2 is always much shorter than τ_1, indicating that the gettering center responsible for the second exponential decay of Fe_i concentration has a higher density than the gettering center which controls the first exponential decay. Hence, the gettering efficiency will rise with the increasing annealing temperature, fully consistent with the observations.

The SIRM technique is used to investigate the defect density and size in all annealed samples and a reference sample which is from the same as-grown wafer and subjected to no intentional Fe introduction and thermal treatments. Each measurement records the scattered light image of a 200 × 200 μm^2 area and 25 separated areas are measured on one sample in order to have enough statistical relevance. It is observed that the defect size and density are nearly constant, independent of the Fe indiffusion and subsequent anneals. Fig. 4(a) shows the average density and size of the defects detected by SIRM in as-grown and 500 °C annealed samples at a depth of 80 μm. It can be concluded that the two experimental points show no difference within the experimental uncertainty. The defect size distribution of the two samples can be fitted well with the Gauss function and also shows little difference as illustrated in Fig. 4(b). The SIRM results indicate that no new defects (that can be observed by SIRM) are created by the Fe drive-in step and subsequent gettering processes. The observed defects are therefore most probably the defects grown-in during crystal pulling that are acting as Fe gettering sites. The defect size obtained in this work is in good agreement with the reported value of void size obtained on as-grown wafers from a similar crystal [16]. Hence, in the present experiments, grown-in voids are most probably one of the gettering centers for interstitial iron while the second type of gettering centers are grown-in oxide precipitates of which the size is below SIRM detection limit.

4. Conclusion

In summary, Fe gettering kinetics in as-grown p-type Cz-Si at low temperatures is investigated. The Fe_i concentration decrease during annealing can be well fitted by a double exponential function, suggesting that there are two types of gettering centers in the as-grown silicon. The contaminated samples and clean sample have similar density and size of grown-in defects that are detected by SIRM. Hence, it is considered that Fe contamination and the anneals are not creating new sinks for Fe_i and the observed gettering is therefore most probably by the defects grown-in during crystal pulling, i.e. about 10^7 cm^{-3} voids

Table 1
Best fitting parameters of the fits in Fig. 3 using Equation (2).

Temperature (°C)	A	τ_1 (h)	τ_2 (h)	Goodness of fit R^2
220	0.77 ± 0.04	179 ± 36	7.8 ± 1.8	0.9788
300	0.61 ± 0.02	90.6 ± 7.8	3.22 ± 0.31	0.9915
400	0.43 ± 0.02	23.2 ± 2.7	0.88 ± 0.07	0.9885
500	0.41 ± 0.02	5.65 ± 0.49	0.33 ± 0.02	0.9973

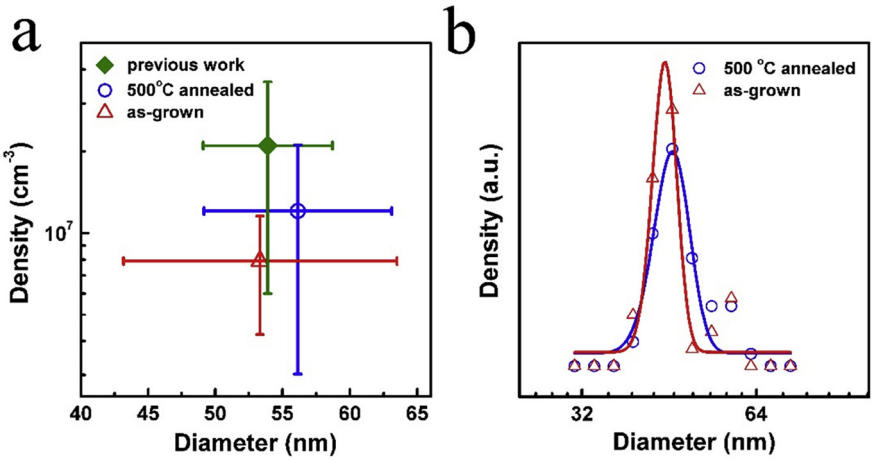

Fig. 4. a: SIRM results obtained on as-grown and 500 °C annealed samples. A previous result obtained on wafers from a similar crystal is shown for comparison [16]. b: The Gauss curve fitting of the size distribution of the observed defects in the two samples.

(that are observed by SIRM) and a several orders of magnitude larger density of oxide precipitate nuclei that are too small to be observed.

Acknowledgements

This work is supported by National Natural Science Foundation of China (Nos. 51532007, 61574124 and 61274057), and Program for Innovative Research Team in University of Ministry of Education of China (IRT13R54).

References

[1] E.R. Weber, Transition metals in silicon, Appl. Phys. A 30 (1983) 1–22.
[2] A.A. Istratov, H. Hieslmair, E.R. Weber, Iron contamination in silicon technology, Appl. Phys. A 70 (2000) 489–534.
[3] A.A. Istratov, H. Hieslmair, E.R. Weber, Iron and its complexes in silicon, Appl. Phys. A 69 (1999) 13–44.
[4] D. Gilles, E.R. Weber, S.K. Hahn, Mechanism of internal gettering of interstitial impurities in Czochralski-grown silicon, Phys. Rev. Lett. 64 (1990) 196–199.
[5] S.A. McHugo, E.R. Weber, M. Mizuno, F.G. Kirscht, A study of gettering efficiency and stability in Czochralski silicon, Appl. Phys. Lett. 66 (1995) 2840.
[6] H. Hieslmair, A.A. Istratov, S.A. McHugo, C. Flink, T. Heiser, E.R. Weber, Gettering of iron by oxygen precipitates, Appl. Phys. Lett. 72 (1998) 1460.
[7] M. Aoki, A. Hara, Re-emission of iron originally gettered by oxygen precipitates in a silicon wafer, J. Appl. Phys. 74 (1993) 1440.
[8] B. Shen, X.Y. Zhang, K. Yang, P. Chen, R. Zhang, Y. Shi, Y.D. Zheng, T. Sekiguchi, K. Sumino, Gettering of Fe impurities by bulk stacking faults in Czochralski-grown silicon, Appl. Phys. Lett. 70 (1997) 1876.
[9] P. Zhang, H. Väinölä, A.A. Istratov, E.R. Weber, Thermal stability of internal gettering of iron in silicon and its impact on optimization of gettering, Appl. Phys. Lett. 83 (2003) 4324.
[10] W.B. Henley, D.A. Ramappa, Iron precipitation in float zone grown silicon, J. Appl. Phys. 82 (1997) 589–594.
[11] F.S. Ham, Theory of diffusion-limited precipitation, J. Phys. Chem. Solids 6 (1958) 335–351.
[12] F.S. Ham, Diffusion-limited growth of precipitate particles, J. Appl. Phys. 30 (1959) 1518–1525.
[13] A. Haarahiltunen, H. Väinölä, O. Anttila, E. Saarnilehto, M. Yli-Koski, J. Storgårds, J. Sinkkonen, Modeling of heterogeneous precipitation of iron in silicon, Appl. Phys. Lett. 87 (2005) 151908.
[14] A. Haarahiltunen, H. Väinölä, O. Anttila, M. Yli-Koski, J. Sinkkonen, Experimental and theoretical study of heterogeneous iron precipitation in silicon, J. Appl. Phys. 101 (2007) 043507.
[15] D. Macdonald, L.J. Geerligs, A. Azzizi, Iron detection in crystalline silicon by carrier lifetime measurements for arbitrary injection and doping, J. Appl. Phys. 95 (2004) 1021.
[16] J. Vanhellemont, X. Zhang, W. Xu, J. Chen, X. Ma, D. Yang, On the assumed impact of germanium doping on void formation in Czochralski-grown silicon, J. Appl. Phys. 108 (2010) 123501.